Lubricant dewetting on the slider's air bearing surface in hard disk drives

Alejandro Rodriguez Mendez, David B. Bogy

Computer Mechanics Laboratory, Department of Mechanical Engineering, University of California, Berkeley, CA 94720, USA

Abstract: In current hard disk drives the minimum air-bearing clearance is of the order of 1 nm during the read/write process. At this ultra-low spacing lubricant from the disk often transfers to the slider's air bearing surface imposing a significant degradation of its performance. It is necessary to make accurate predictions of the lubricant's response at the head-disk interface in order to engineer reliable hard disk drives. In this article we perform numerical simulations to investigate the dewetting behavior of some perfluoropolyether lubricant films used in hard disk drives. We model the lubricant flow on the slider surface using a governing equation based on classical lubrication theory. We consider a disjoining pressure that approximates the properties of a ZTMD lubricant and compare the results with those obtained using a purely van der Waals disjoining pressure. We study the spreading of a lubricant film on a slider both at rest and while flying over a spinning disk. The effect of surface tension, air shear stress and substrate roughness on the dewetting behavior of the film is also investigated.

1. Introduction

In order to achieve higher recording densities in a hard disk drive (HDD) the read/write head should be brought closer to the disk. Currently, the minimum air-bearing clearance in HDDs is between 1 and 2 nm [1]. At this ultra-low spacing lubricant from the disk often transfers to the slider's air bearing surface (ABS) forming a molecularly thin film that imposes a significant degradation of its performance [2-3]. To achieve the future required sub-nanometer clearances, perturbations in the lubricant film need to be kept to less than a few angstroms in thickness [4]. Consequently, it is important to make accurate predictions of the lubricant response at the head-disk interface in order to engineer reliable HDDs. Lubricants used in current HDDs have reactive functional end groups that bond the lubricant to the disk protective carbon overcoat [5-6]. When these lubricant films reach a critical thickness they become unstable and form either multilayers or droplet structures [7-10]. The above unstable phenomenon on liquid films is known as dewetting. Generally, dewetting describes the rupture of a thin liquid film on the substrate and the formation of droplets [11-15].

To accurately predict the motion of lubricants in a HDD it is necessary to have a proper understanding of the lubricant's thin film properties. An important property to consider is the lubricant's disjoining pressure. It is observed experimentally that in nanometer-thin lubricant films, the molecules in the solid substrate interact with those of the coating fluid giving rise to an additional pressure within the liquid film (additional to that induced by surface tension and ambient pressure). This pressure is known as disjoining pressure. Disjoining pressure is generated by several molecular interactions such as: van der Waals forces, electrostatic forces between charged surfaces, structural effects of the liquid; this last force arises due to molecules within the film having a structure different from that of the bulk lubricant [16]. Disjoining pressure characterizes the state of a thin layer. The pressure depends on the thickness of the film, the composition and properties of the interacting bodies, and their temperature. In the lubrication approximation, when the slope of the free surface of the film is small compared to unity, we can assume that the outcome of all interactions between the film and the exterior environment is a pressure, $\Pi(h)$, which depends only on the local film thickness h. The disjoining pressure $\Pi(h)$ can be either positive (solid substrate repels the air-liquid interface) or negative (solid substrate attracts the air-liquid interface), depending on the properties and thickness of the solid substrate and coating films [17]. We can interpret the disjoining pressure to be an external pressure in addition to that of the air pressure acting on the air-liquid interface.

The behavior of nanoscale thin films is determined mainly by their disjoining pressure. Most studies in HDDs consider a disjoining pressure due only to van der Waals forces which results in the expression, $\Pi(h) = Ah^{-3}$. This model provides only a crude estimate for the spreading of lubricant on the slider surface. It cannot predict the motion of liquid films where multilayer or dewetting formations occur.

In this article we perform numerical simulations to investigate the dewetting behavior of some perfluoropolyether (PFPE) lubricant films used in HDDs. We model the lubricant flow on the slider surface using a governing equation based on classical lubrication theory from fluid mechanics. A disjoining pressure that approximates the properties of a typical PFPE lubricant used in current HDDs is considered. Using this disjoining pressure we obtain conditions under which dewetting of the film occurs. We obtain results for lubricant flow and reflow on the

slider's ABS when the HDD is operating and at rest, respectively. The effect of substrate roughness on the dewetting behavior of the film is also taken into account.

2. Governing equation for the film thickness

In current HDDs, the lubricant film coating the surface of the disk consists of only a few molecules across its thickness [18-21]. However, it has been shown that the dynamics of these films can be well described by the theory of continuum mechanics, which yields adequate results when compared with experiments [22-23]. Within the continuum framework, the dimensions of the film and the conditions of operation of the HDD make suitable the use lubrication theory to obtain governing equations for the flow on the slider's surface [24-26]. Following the analysis carried out in [24], we obtain a partial differential equation that describes the time evolution of the lubricant thickness on the slider's ABS. This equation is given by,

$$h_t + \nabla \cdot \left\{ \frac{h^2}{2\mu} \boldsymbol{\tau} - \frac{h^3}{3\mu} \nabla [p - \sigma \Delta h - \Pi(h)] \right\} = 0, \tag{1}$$

where $h(x, y, t), \mu, p, \sigma,$ and $\Pi(h)$ are the lubricant thickness, lubricant viscosity, air pressure, surface tension and disjoining pressure, respectively. The term $\boldsymbol{\tau} = \left(T_{xz}, T_{yz}\right)$ is the air shear stress vector at the slider's surface. The symbols $\nabla, \nabla \cdot$ and Δ represent the two dimensional (*x*, *y*) gradient, divergence and Laplace operators. The *x*, *y*, *z* coordinates correspond to the directions along the slider's length, the slider's width and the lubricant thickness, respectively. It is convenient to non-dimensionalize equation (1) to obtain relative scales for all the terms involved in it. For this purpose we replace the dimensional variables $h, t, x, y, \boldsymbol{\tau}, p, \Pi$ by the non-dimensional ones $h_0 h, t_s t, Lx, Ly, \tau_s \boldsymbol{\tau}, p_s p, \Pi_s \Pi$ where $h_0, t_s, L, \tau_s, p_s, \Pi_s$ are referential values for their corresponding variables. We take $\Pi_s = \Pi(h_0)$ and assume that the referential values h_0, L, p_s are known from the characteristics of the HDD. Then, evident choices for the remaining scales are $\tau_s = 2h_0 p_s/(3L)$ and $t_s = 3\mu L^2/(h_0^2 p_s)$. With these choices we obtain the non-dimensional equation,

$$h_t + \nabla \cdot \{h^2 \boldsymbol{\tau} - h^3 \nabla [p - C_\sigma \Delta h - C_\pi \Pi(h)]\} = 0, \tag{2}$$

where $C_\sigma = \sigma h_0/(p_s L^2)$, and $C_\pi = \Pi_s/p_s$. Typical scales for a PFPE lubricant film in a HDD are: $h_0 = 1\, nm, L = 1\, mm, \mu = 1\, Pa \cdot s, \sigma = 0.02\, N/m\,, p_s = 100\, kPa, \Pi_s = 1\, \mathrm{M}Pa$ [20, 26-29]. Hence, we obtain the coefficients $C_\sigma = 2(10^{-10})\,, C_\pi = 10$. Therefore, for these length scales we observe that the surface tension effect is negligibly small compared to the other terms in (2) and thus can be neglected. This assumption is also found elsewhere in the literature [30].

We want to use a model for disjoining pressure that characterizes the behavior of a PFPE lubricant film used in HDDs. For this purpose we consider the disjoining pressure model proposed by [31] which takes into account van der Waals, electrostatic and structural intermolecular forces. This model, which we call *structural disjoining pressure*, roughly approximates the behavior of a ZTMD lubricant and is described by,

$$\Pi(h) = a_1 h^{-3} + a_2 e^{-a_3 h} + a_4 \cos(a_5 h + a_6)\, e^{-a_7 h}, \tag{3}$$

with $a_1 = (10^{-19})/(6\pi)\,Nm$, $a_2 = -1.6(10^6)\ N/m^2$, $a_3 = 5(10^8)$, $a_4 = -10^6\ N/m^2$, $a_5 = 1.57(10^9)$, $a_6 = 3.77$, $a_7 = 2.5(10^8)$ [31]. We want to compare the results obtained using (3) with those obtained using the purely *van der Waals disjoining pressure* given by,

$$\Pi(h) = a_1 h^{-3}, \tag{4}$$

where a_1 is known as the Hamaker constant. An example of a commercial lubricant with a purely van der Waals disjoining pressure is Fomblin-Z [32]. To show the effect of the disjoining pressure on the lubricant behavior we consider a third model which is composed of an attractive and a repulsive term. We call this model the *two-term disjoining pressure* which is given by

$$\Pi(h) = -a_1 h^{-3} + a_8 h^{-4}, \tag{5}$$

with $a_8 = 6(10^{-30})\ Nm^2$ [33]. This model of disjoining pressure roughly approximates the behavior of the commercial ZDOL lubricant within the region $0 < h < 5$ [34]. The disjoining pressure models (3), (4) and (5) are plotted as a function of lubricant thickness in Fig. 1.

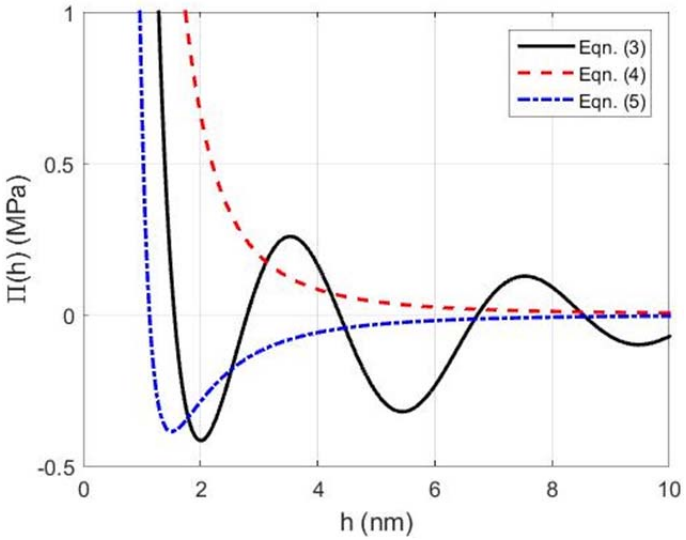

Fig. 1. Disjoining pressure as function of film thickness given by equations (3), (4) and (5).

Equation (1) is known to be unstable for certain values of the disjoining pressure and its derivative [33]. In particular, if we linearize (1) around $h = h_0$ and assume that the disjoining pressure term is dominant, so that all other terms can be neglected, we are left with $h_t + k\Delta h = 0$, where $k = h_0^3\Pi'(h_0)/(3\mu)$. This equation is the ubiquitous heat equation, which is known to be stable for $k \leq 0$, i.e. when $\Pi'(h_0) \leq 0$ and unstable when $k > 0$, i.e. when $\Pi'(h_0) > 0$ [35]. For the structural disjoining pressure given by (3), when the thickness h is less than 2 nm, $\Pi'(h) \leq 0$, so we expect the film to be stable within this range. On the other hand, when h is just above 2 nm we have $\Pi'(h) \geq 0$, hence dewetting of the film is expected to occur. Similarly, for the two-term disjoining pressure given by (5) we expect dewetting of the film when the thickness h is larger than 1.5 nm. Also, the lubricant film is stable for all values of h when the disjoining pressure is determined by (4).

Lubricants, Fomblin-Z, ZDOL and ZTMD, represented roughly by the disjoining pressure models (4), (5) and (3), have the same perfluoropolyether (PFPE) backbone and an increasing number of hydroxyl functional end groups per molecule: 0, 2, and 8 respectively [20]. The polymer backbone for these lubricants is of the form $-(OCF_2CF_2)_n-(OCF_2)_m-O-$ where m/n=1.2 [36]. As the number of hydroxyl end groups on the polymer backbone is increased from zero to eight, the viscosity of the thin lubricant film increases as well [20]. However, in this paper we focus attention only on the effect of the disjoining pressure model and thus consider the same value of viscosity for the three models described above. A detailed description of these lubricants and their properties can be found elsewhere [5, 20, 36].

It is known that the viscosity of a thin film can differ significantly from its bulk value, i.e. the viscosity is thickness dependent [27]. Therefore, throughout this paper we chose the value of viscosity $\mu = 1\ Pa \cdot s$ corresponding approximately to a film thickness of 2 nm for ZTMD at 100 °C [26]. We simplify the analysis by considering the viscosity to be constant (independent of film thickness).

3. Lubricant flow on the slider's air bearing surface

We next simulate the lubricant flow on a slider's air bearing surface. We consider a slider with the ABS design shown in Fig. 2. The length and width of this slider are L = 1.33 mm and W = 0.83 mm respectively.

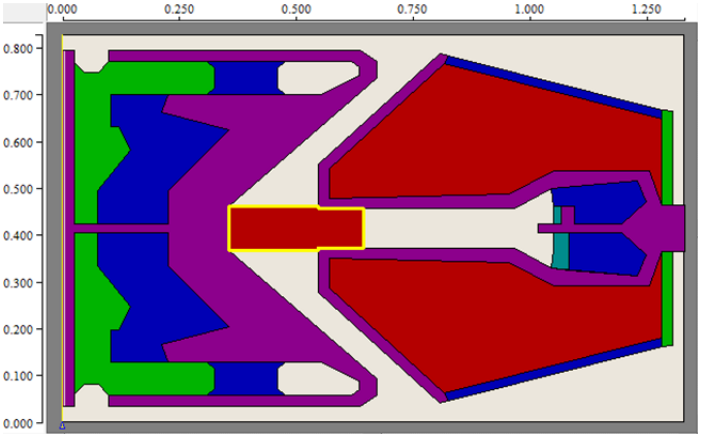

Fig. 2. Air bearing surface design used in the simulations. The length and width of this slider are L = 1.33 mm and W = 0.83 mm respectively.

We consider the slider when it is flying over a disk spinning at 10,000 rpm. The slider is located on a disk track at a radius of 23 mm with zero skew angle. Then, the steady state flying attitude for the slider shown in Fig. 2 is: minimum flying height = 12.28 nm, pitch angle = 135.7 μrad, roll angle = 15.96 μrad. These values as well as the air shear stress and air bearing pressure are calculated using the CMLAir air bearing solver [37]. In order to study the lubricant accumulation outside the ABS using the two-dimensional model (2), we unfold the slider's trailing edge lateral wall, also known as deposit end, placing it on the same plane with the ABS. The air shear stress and air pressure gradient are set to zero on the deposit end; hence the lubricant flow in the deposit end is driven only by disjoining pressure. As initial condition, we consider that the slider surface and deposit end are coated with a uniform 1 nm lubricant film. We solve equation (2) using an implicit finite difference numerical scheme with second order accuracy. As boundary

conditions we set the restriction $\partial h/\partial n = 0$ on the four outer edges; this condition is equivalent to imposing a zero volume flux through any of the boundaries. We use the structural disjoining pressure (3) and compare the results with those obtained using the purely van der Waals disjoining pressure (4). The simulation results are presented in Fig. 3, where the area to the left of the vertical black line is the ABS location and the area to the right denotes the deposit end.

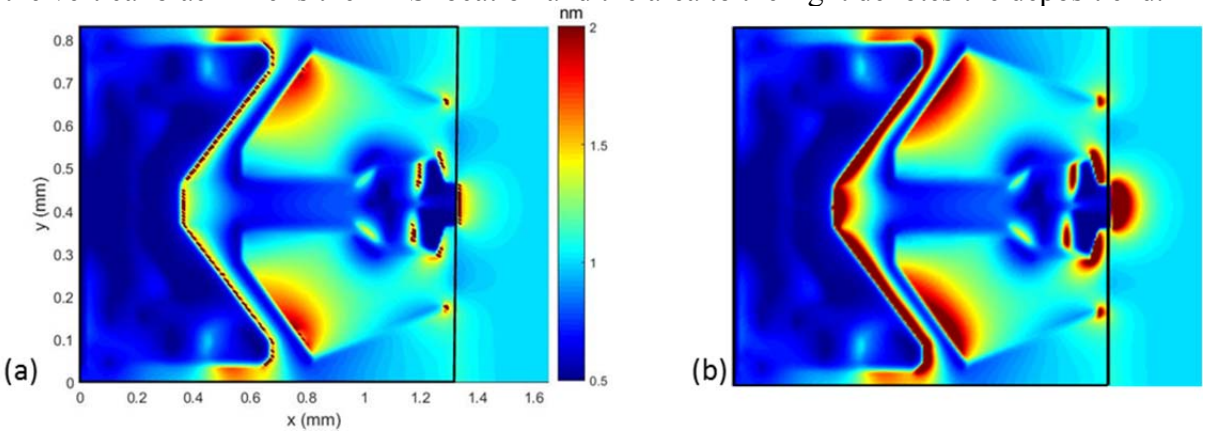

Fig. 3. Thickness profile on the ABS and deposit end at time t = 100 s for a film with (a) structural disjoining pressure (3) and (b) van der Waals disjoining pressure (4). The film thickness shown can be larger than 2 nm in some locations; however the plots were trimmed at 2 nm to obtain a more detailed view of the lubricant profile. The area to the left of the vertical black is the ABS location and the area to the right is the deposit end location.

The results obtained using the purely van der Waals disjoining pressure (4) are considerably different from those obtained with the structural disjoining pressure (3). As shown in Fig. 3b, after a time of 100 s, the lubricant thickness is larger than 2 nm on certain locations of the ABS without dewetting occurring. On the other hand, in Fig. 3a it is observed that as the air shear stress forces the lubricant to migrate and accumulate at various places on the surface of the slider, the film becomes unstable at those regions where its thickness h is such that $\Pi'(h) > 0$. There, the film breaks up into droplets. As time progresses, the droplets increase in height and decrease in width. Eventually, the width of the droplets narrows down to the size of the computational grid ($2.5\ \mu m$) at which point the solution is no longer valid. Since the surface tension effect is negligibly small at this length scale, there is no opposing force to balance the action of the disjoining pressure and air shear stress. Therefore, the droplets continue to grow unboundedly. However, we expect that as the droplets widths decrease, the magnitudes of their curvatures will be sufficiently large for surface tension to become important. This can only happen at a smaller length scale, of the order of $1\ \mu m$.

The results presented in Fig. 3 correspond to the particular slider design shown in Fig. 2. However, a similar behavior on different ABS designs is expected, i.e. a relatively large accumulation of lubricant may be found on recessed cavities, around the central trailing pad and on the deposit end. In these areas, when the lubricant thickness h increases to a value such that $\Pi'(h) > 0$, then dewetting of the film is expected to occur.

4. Dewetting of a lubricant film with non-negligible surface tension effect

We consider next a computational domain of magnitude $L \times W = 1\ \mu m \times 1\ \mu m$, which represents a small portion of the slider's ABS. If we use a computational grid size of 5 nm and use this as the length scale for equation (2), then the coefficient of the surface tension term in (2)

becomes $C_\sigma = 8$. Thus, the magnitude of surface tension is significant in this case and its effect balances that of the disjoining pressure.

We first study the spreading of a lubricant film when the HDD is at rest, i.e. when the slider is not flying over the disk. In this condition, the air shear stress and air pressure gradient vanish. Therefore, equation (1) can be simplified, and after non-dimensionalization we obtain,

$$h_t + \nabla \cdot \{h^3 \nabla[\Delta h + \Pi(h)]\} = 0, \tag{6}$$

where we have replaced h, t, x, y, Π in (1) by the non-dimensional variables $h_0 h, t_s t, Lx, Ly, \Pi_s \Pi$ and used $t_s = 3\mu L^4/(\sigma h_0^3)$, $\Pi_s = \sigma h_0/L^2$ so that the surface tension term balances the disjoining pressure term. We solve this equation numerically using as boundary conditions the restrictions $\partial h/\partial n = 0$ and $\partial^3 h/\partial n^3 = 0$ on the four walls; this condition is equivalent to imposing a zero volume flux through the outer boundaries. We use the lubricant properties $\sigma = 0.02\ N/m$ [28], $\mu = 1\ Pa \cdot s$.

We first study the spreading of a uniform lubricant layer with an initial thickness of 2.5 nm. In the middle of the domain we create a 1 nm deep hole to act as a perturbation of the film as seen in Fig. 4 (0 s). We choose the two-term disjoining pressure model given by equation (5). The simulation results are shown in Fig. 4.

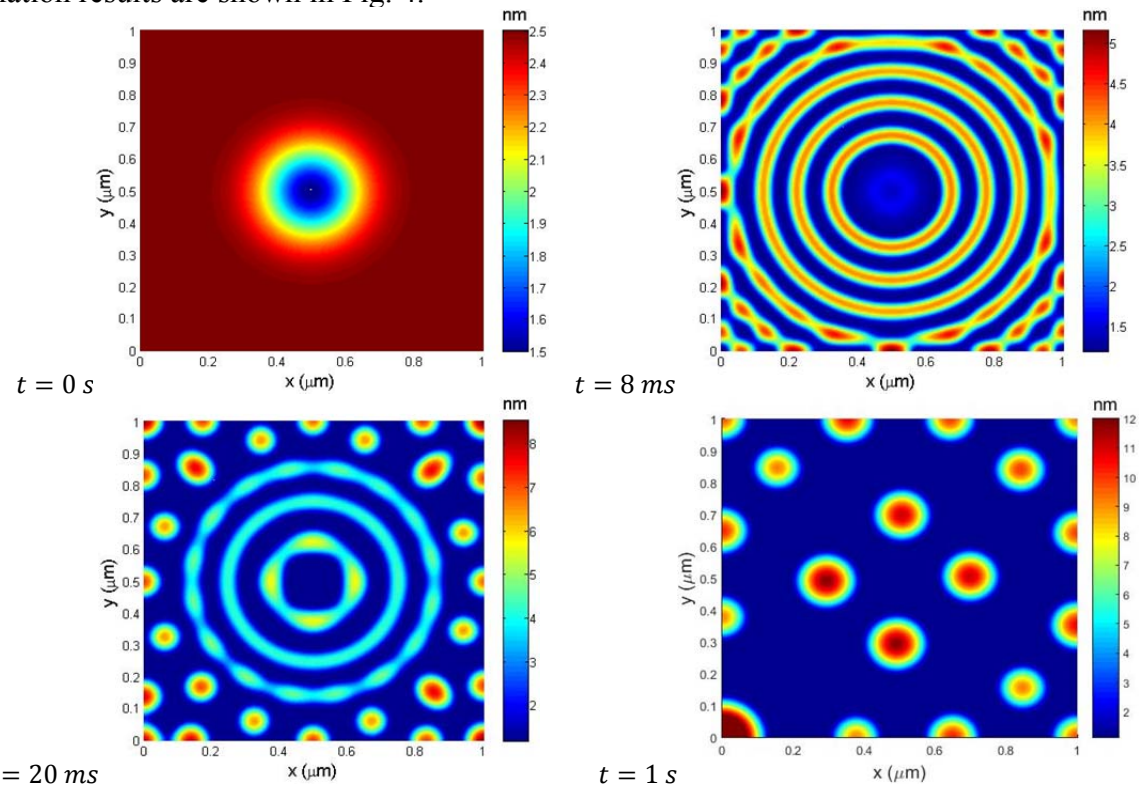

Fig. 4. Thickness profiles of the spreading of a uniform film with a center hole at times 0 s, 8 ms, 20 ms, and 1 s, using the two-term disjoining pressure model given by (5).

From Fig. 4 (0 s), we observe that the film initially has a thickness larger than 1.5 nm so that $\Pi'(h) > 0$. This implies that the state of the film is unstable. The center hole increases in width as time progresses generating concentric rings around it which eventually break up into droplets

as seen in Fig. 4 (8 ms and 20 ms). The droplets merge with each other to form larger ones which continue to grow until their curvature is large enough for the surface tension effect to balance the disjoining pressure. At time t = 1 s, the state of the lubricant is that of a few isolated droplets connected by a uniform film with a thickness of 1.16 nm, approximately the value of h at which $\Pi(h) = 0$ and $\Pi'(h) < 0$ as observed in Fig. 1, Eq. (5). The largest droplet has a maximum thickness of 11.8 nm and is surrounded by other droplets of equal or smaller thickness.

Now consider a lubricant with the structural disjoining pressure given by (3). Assume the same initial condition used above, i.e. a uniform 2.5 nm film with a center hole, 0.2 μm wide and 1 nm deep. In this case the initial film is already unstable since $\Pi'(h) > 0$ when $h > 2\,nm$. The results are shown in Fig. 5.

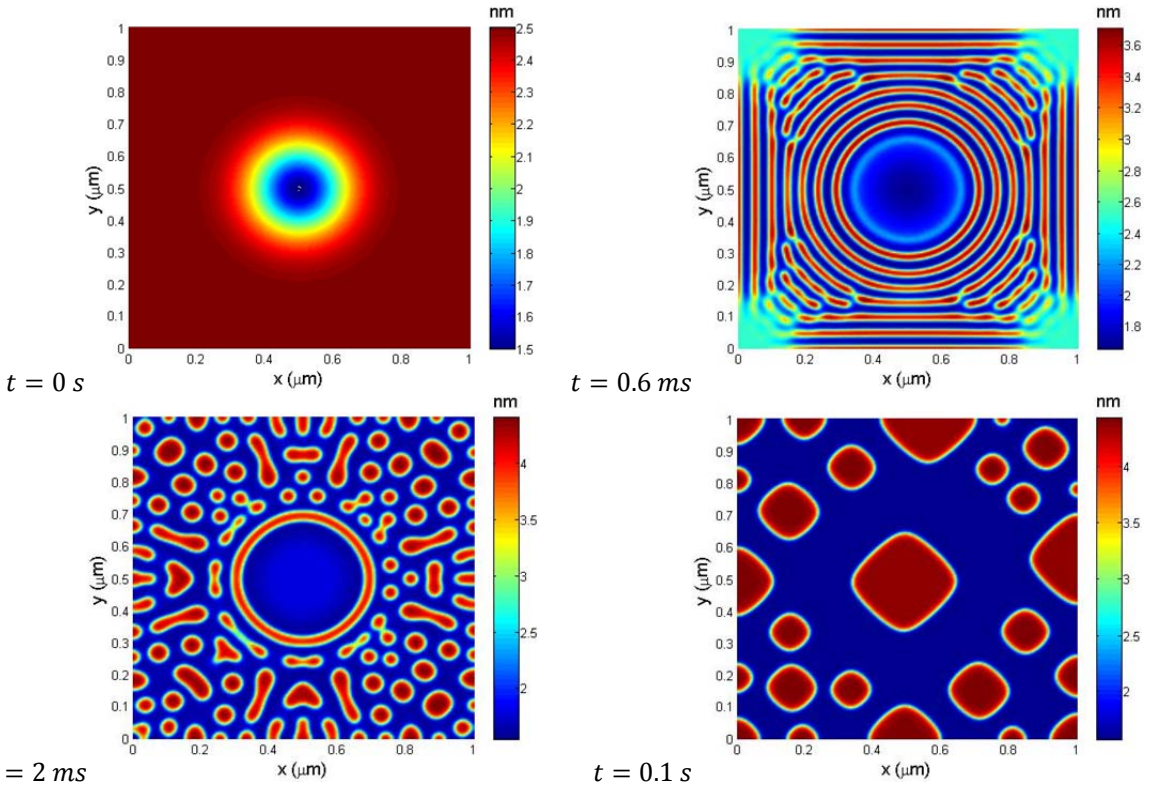

Fig. 5. Thickness profiles of the spreading of a uniform film with a center hole at times 0 s, 0.6 ms, 2 ms, and 0.1 s, using the structural disjoining pressure model given by (3).

The process of dewetting seen in Fig. 5 using the structural model (3) is similar to that shown in Fig. 4 where we used the two-term model (5). As the center hole increases in width it generates rings of lubricant around it which are circular in the interior of the domain and square shaped near the boundaries as seen in Fig. 5 (0.6 ms). The rings reach the boundary first at the center of the walls and eventually break up into small droplets that coalesce into larger ones as seen in Fig. 5 (2 ms). At time t = 0.1 s the state of the film consists of a few isolated droplets, all of which have a thickness of 4.4 nm and are connected by a uniform 1.5 nm film. The thickness of the droplets and of the connecting film corresponds to those values of h at which $\Pi(h) = 0$ and $\Pi'(h) < 0$ as observed in Fig. 1, Eq. (3). The thickness of all droplets never exceeds a value of 4.4 nm in contrast to the results obtained using the two-term model (5). The droplets shown in Fig. 5 (0.1 s) have a rectangular shape with a flat top. On the other hand, those droplets observed

in Fig. 4 (1 s) have circular shapes with spherical caps. For this reason we will refer to the droplets shown in Fig. 5 (0.1 s) as *islands*. On the flat top of these islands, the surface curvature and disjoining pressure are both zero so the term inside brackets in equation (6) vanishes as well as its gradient since the film thickness on the top of the islands is constant. The disjoining pressure derivative $\Pi'(h)$ on both the connecting film and on the islands is negative which, as observed in section 3, favors the stability of the film.

If enough lubricant is deposited on the slider surface, the spherical droplets shown in Fig. 4 may continue to merge and grow to thicknesses over 100 nm as found experimentally in [38] becoming a potential risk to the tribological performance of the HDD. The largest droplets can drop off the slider onto the disk surface where they act effectively as asperities. When the slider flies over these lubricant asperities they may induce undesirable oscillations of the slider degrading the HDDs read/write performance. On the other hand, the islands shown in Fig. 5 may continue to merge forming a 4.4 nm lubricant layer over the slider surface which, when the slider is flying over the disk, it may induce an increase in air bearing spacing degrading the magnetic signal of the HDD as found experimentally in [22].

5. Effect of substrate roughness

We now investigate the effect of substrate roughness on the dewetting behavior of the lubricant. For this purpose we consider a substrate roughness with a maximum peak value of 0.1 nm. The roughness was generated randomly using a Gaussian noise distribution and is depicted in Fig. 6.

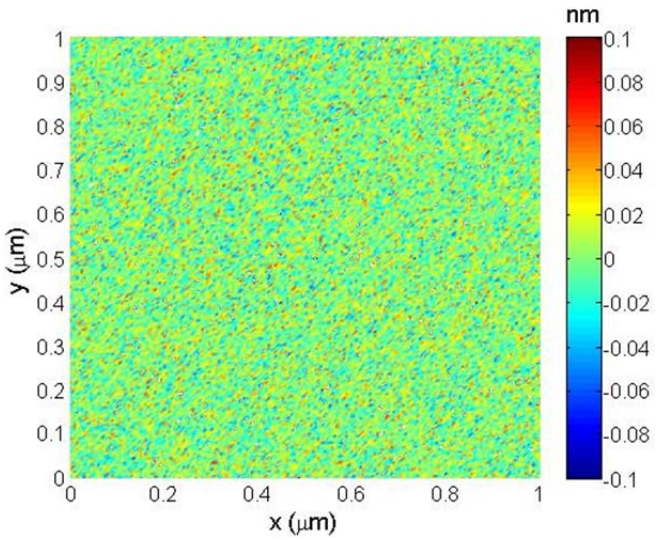

Fig. 6. Substrate roughness generated by Gaussian noise with maximum peak value of 0.1 nm.

On top of the substrate roughness we consider a lubricant film with a uniform thickness of 2.5 nm relative to the mid-plane of the substrate roughness. We use the structural disjoining pressure model given by (3). The results are presented in Fig. 7.

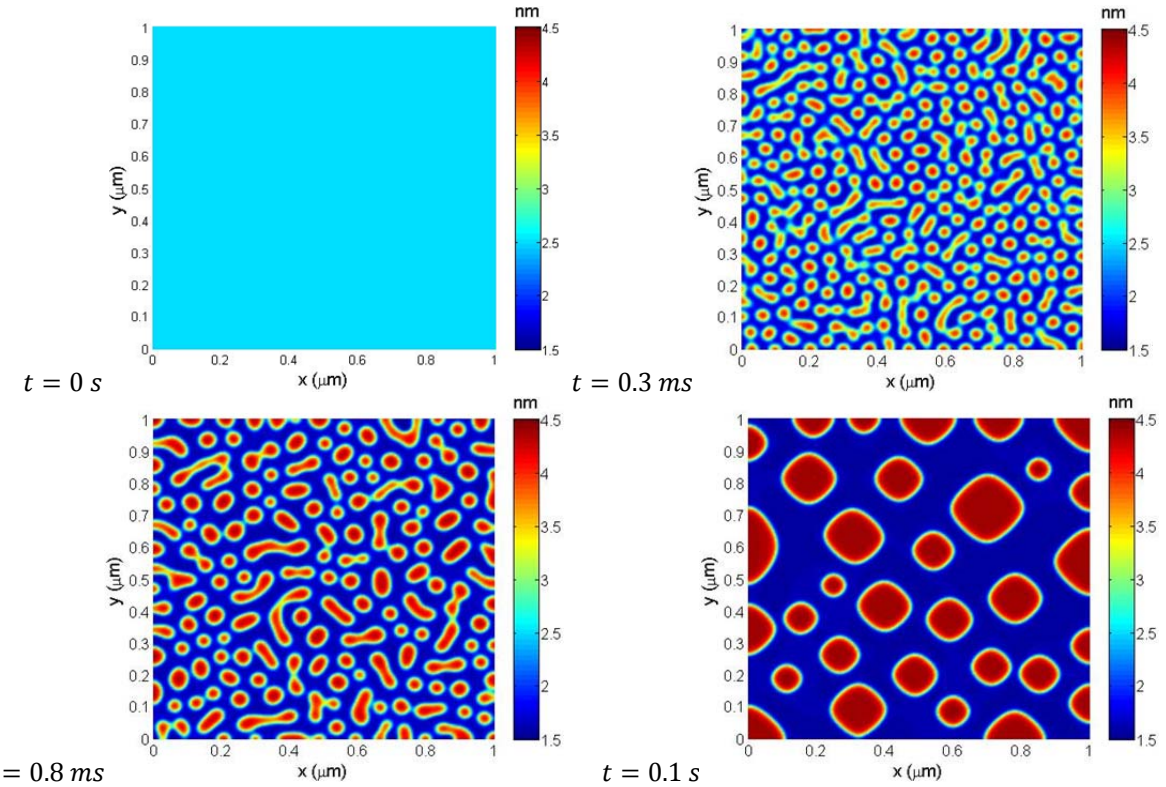

Fig. 7. Thickness profiles of the spreading of a uniform film coating a substrate with roughness at times 0.15 ms, 0.3 ms, 0.8 ms, and 0.1 s, using the structural disjoining pressure model given by (3). The thickness shown is relative to the substrate's mid-plane.

As observed in Fig. 7 the substrate roughness induces the uniform film to break up into droplets distributed throughout the computational domain. As time progresses, the smaller droplets merge with each other to form larger ones. After a time t = 0.1 s the state of the film consists of a few islands droplets with thicknesses of around 4.4 nm connected by a uniform 1.5 nm film. As observed above, the connecting film and island thickness correspond to the values of h at which $\Pi(h) = 0$ and $\Pi'(h) < 0$. The film thickness reaches a minimum and maximum value of 1.5 nm and 4.4 nm in approximately 0.5 ms. However, when the film has a single disturbance such as the case shown in Fig. 5, (or when the substrate is smooth with only a single 0.1 nm asperity) the film thickness reaches the limit values, 1.5 nm and 4.4 nm, in 1.5 ms. Therefore, the dewetting process is three times faster on a rough substrate than on a semi-smooth substrate. We note that a uniform film on a perfectly smooth substrate does not dewet since all partial derivatives in equation (6) vanish in this case and the film remains uniform for all time t. At a time of 0.1 s, a larger number of islands is observed on the rough substrate, as shown Fig. 7, than on the smooth substrate shown in Fig. 5. We also observe that initially the lubricant thickness increases on the low points of the substrate and decreases on the high points of the substrate. This process continues until the lubricant thickness reaches the limit values of 4.4 nm and 1.5 nm.

6. Effect of air shear stress and air pressure

Now consider the spreading of a lubricant film when the HDD is operating, i.e. when the slider is flying over the spinning disk. In this case, we must consider the effects of air shear stress and air pressure. Since the dimensions of the computational domain have a size of $1\ \mu m \times 1\ \mu m$ and the air shear stress and air pressure gradient vary on a scale of the order of $1\ \mu m$, they can be

considered constant on such length scales, i.e. $\boldsymbol{\tau}$ and ∇p are constant in this case. With this assumption, the governing equation (1) can be written in the following non-dimensional form,

$$h_t + \nabla \cdot \{h^3 \nabla[\Delta h + \Pi(h)]\} + \boldsymbol{d} \cdot \nabla h = 0, \tag{7}$$

where $\boldsymbol{d}(h) = (2h\boldsymbol{\tau} - 3h^2\nabla p)$. To obtain (7) we have replaced $h, t, x, y, \boldsymbol{\tau}, p, \Pi$ in (1) by the non-dimensional variables $h_0 h, t_s t, Lx, Ly, \tau_s \boldsymbol{\tau}, p_s p, \Pi_s \Pi$ and chosen $\tau_s = 2\sigma h_0^2/(3L^3)$, $t_s = 3\mu L^4/(\sigma h_0^3)$, $p_s = \sigma h_0/L^2$, $\Pi_s = \sigma h_0/L^2$. As before, the air shear stress and air pressure gradient are calculated using the CMLAir solver [37]. We choose a location on the central trailing edge pad of the slider shown in Fig. 2. There we obtain the values $\boldsymbol{\tau} = (22.5\, kPa, 0)$ and $\nabla p = (-1.5(10^{11})\ N/m^3, 0)$. We solve equation (7) numerically using the same boundary conditions used in section 4.

We consider two different initial conditions. The first condition is the one shown in Fig. 4 (0 s), i.e. a lubricant droplet, 2.5 nm thick and 0.2 μm wide, in the center of a uniform 1.5 nm thick film. For this condition we use the two-term disjoining pressure (5) to obtain the results shown in Fig. 8a. The second condition is the one shown in Fig. 5 (0 s), i.e. a uniform 2.5 nm film with a center hole, 0.2 μm wide and 1 nm deep. For this condition we use the structural model disjoining pressure (3) to obtain the results shown in Fig. 8b.

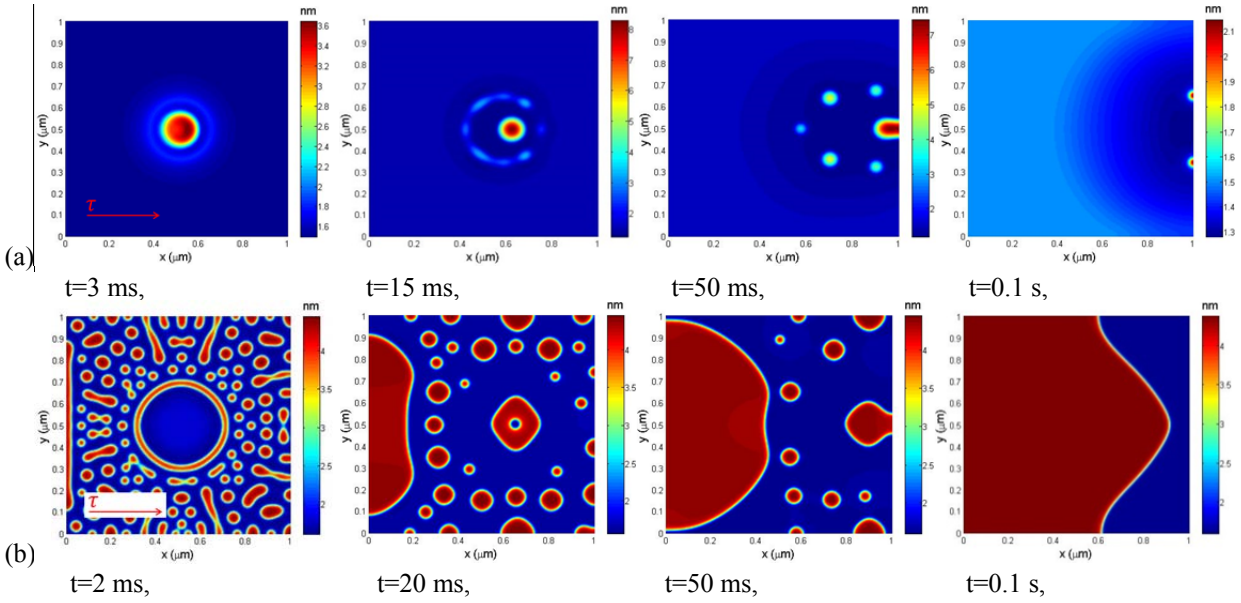

Fig. 8. Thickness profiles of the spreading of two lubricant films under the action of air shear stress and air pressure gradient. (a) Two-term disjoining pressure (5). The initial condition is a lubricant droplet, 2.5 nm thick and 0.2 μm wide, in the center of a uniform 1.5 nm film. (b) Structural disjoining pressure (3). The initial condition is a uniform 2.5 nm film with a center hole, 0.2 μm wide and 1 nm deep.

From Fig. 8a we observe that the initial droplet has a thickness larger than 1.5 nm so that $\Pi'(h) > 0$. This implies that the state of the droplet is unstable so it starts to increase in thickness and decrease in width. This process continues until the curvature of the droplet is large enough for surface tension to balance disjoining pressure. The initial droplet generates a ring of lubricant around it that eventually breaks up into smaller droplets that are then sheared downstream by the action of the air shear stress and air pressure gradient, in the direction of

vector $\boldsymbol{d}$ in (7). When the droplets reach the right boundary, they start to flatten out until the film becomes almost uniform at time t = 0.1 s.

From Fig. 8b we observe that the center hole increases in width as time progresses generating concentric rings around it that eventually break up into droplets in a similar fashion as the results shown in Fig. 5. The small droplets merge into larger ones forming islands that are sheared downstream in the direction of $\boldsymbol{d}$. The merging process is enhanced by the effect of air shearing. After a time of 0.1 s all the islands have merged into a single one as observed in Fig. 8b (0.1 s). The thickness of the islands and the connecting film correspond approximately to those values of h at which $\Pi(h) = 0$ and $\Pi'(h) < 0$, i.e. 4.4 nm and 1.5 nm. During the dewetting process, the thickness of all islands never exceeds a value of 4.4 nm.

From the results shown in Fig. 8b, we observe that a lubricant film on the slider surface breaks up into many islands. When the slider is flying over the disk surface, the air shear stress $\boldsymbol{\tau}$ brings the islands closer to each other until they merge forming a larger island which can effectively be viewed as a uniform 4.4 nm layer coating the slider's ABS. As indicated in section 4, a lubricant film covering the slider's read/write elements induces an increase in air bearing spacing, thus degrading the magnetic signal of the HDD [22].

7. Spreading of a step on a lubricant film

Next we consider the unforced spreading of a lubricant step of thickness 20.66 nm in its high part and 1.5 nm in its low part as shown in Fig 9a. For disjoining pressure we use the structural model given by (3). The lateral dimensions of the computational domain are chosen to be $L \times W = 1\ mm \times 1\ mm$, similar to those of the slider shown in Fig. 2. We solve equation (6) numerically using the boundary conditions described above. The simulation results are shown in figure 9b.

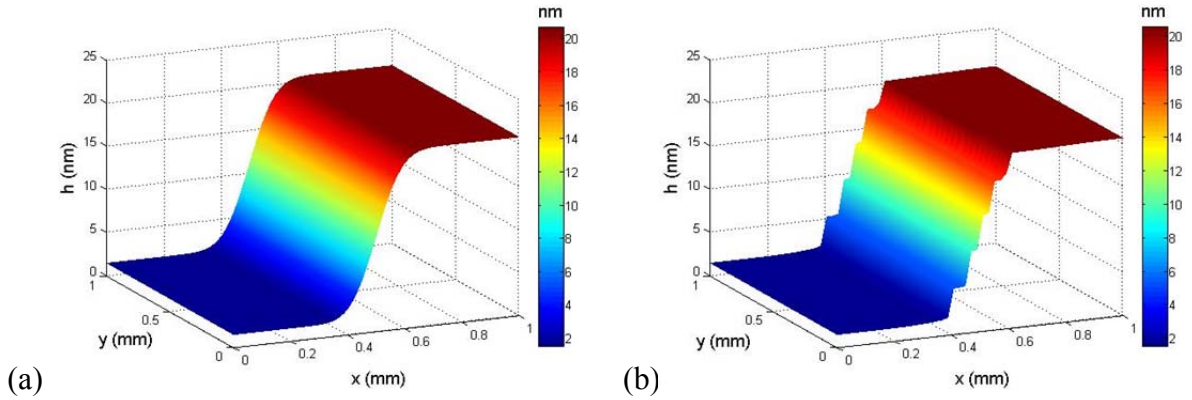

Fig. 9. Lubricant thickness profiles for the spreading of a step on the film at time (a) 0 s and (b) 1000 s, using the structural disjoining pressure (3).

Due to the relatively large lateral dimensions of the slider, relative to the lubricant thickness, surface tension effects are negligible in this case when compared to disjoining pressure effects. As observed in Fig. 9b, after a time of 1000 s the initial lubricant step deforms into a terraced structure. This multilayer structure contains 6 visible layers (5 steps). The first layer has a thickness of 1.5 nm, whereas the height of the next layers is: 4.33 nm, 8.53 nm, 12.64 nm, 16.65 nm and 20.47 nm respectively. These heights correspond closely to those values of h in Fig. 1 at

which $\Pi'(h) < 0$ and $\Pi(h) = 0$ i.e. the thicknesses: 1.55 nm, 4.37 nm, 8.52 nm, 12.59 nm, 16.63 nm and 20.66 nm respectively.

Similar terraced structures as the one shown in Fig. 9b have also been observed in experiments carried out on PFPE lubricants [10]. The development of such a layered structure has been interpreted as a manifestation of a specific molecular conformation. As noted in [10], the first layer develops from the diffusion of molecules within the first monolayer, with end-groups orienting preferentially towards the carbon surface. The interactions between these molecules and the carbon surface are stronger than the intermolecular interactions within the fluid. The second layer is less mobile and exhibits a sharp step which has a thickness nearly twice of the first layer.

8. Conclusions

The dewetting behavior of a PFPE lubricant film on the slider's air bearing surface was investigated. It was observed that, when the lubricant flow is analyzed over the entire air bearing surface, the length scale of the slider is several orders of magnitude larger than the thickness of the film so that surface tension effects are negligible. Under this condition, the air shear stress and disjoining pressure act as the only driving forces during the spreading of a lubricant droplet. When the thickness of the droplet is larger than the critical dewetting thickness, the disjoining pressure is a destabilizing force that induces the unrestrained growth of the film. The film on the slider breaks up into droplets that increase in height and decrease in width. We expect that as this process continues until the curvature of each droplet will be of such significant magnitude that the surface tension will not be negligible any more.

When we consider a portion of the slider with a size of $1\ \mu m \times 1\ \mu m$, the surface tension effect is of significant magnitude so that it balances the effect of disjoining pressure. In this case, an initial lubricant film with a thickness larger than the critical dewetting thickness breaks up into small droplets that then merge into larger ones. The film breaks up almost everywhere when substrate roughness is taken into account. The final state is that of a few stable droplets connected by a uniform film. When we include the effect of air shear stress and air pressure gradient the result is that of an initial film breaking up into droplets which are then merged and sheared downstream in the direction of the air shear stress.

Due to the oscillatory profile of the disjoining pressure used in our simulations, a sharp step on the lubricant film evolves with time into a terraced structure that has been observed in experiments carried out on PFPE lubricants. The thickness of each layer on the terrace is completely determined by the characteristics of the lubricant disjoining pressure. It can be concluded from this analysis that the choices of disjoining pressure models, the nondimensionalization, and the size of the computational domain are all important for capturing experimentally observed phenomena of lubricant behavior in the head-disk interface of hard disk drives.

9. References

[1] Marchon, B., Olson, T. (2009). Magnetic spacing trends: from LMR to PMR and beyond. IEEE Trans. Magn. 45(10), 3608–3611.

[2] Pan, D., Ovcharenko, A., Yang, M., Radicati, F., Talke, F. E. (2014). Effect of pitch and roll static angle on lubricant transfer between disk and slider. Tribology Letters, 53(1), 261-270.
[3] Seo, Y. W., Pan, D. Z., Ovcharenko, A., Yang, M., Talke, F. E. (2014). Molecular Dynamics Simulation of Lubricant Transfer at the Head-Disk Interface. Magnetics, IEEE Trans. Magn. 50(11), 1-4.
[4] Ma, X., Chen, J., Richter, H. J., Tang, H., Gui, J. (2001). Contribution of lubricant thickness to head-media spacing. Magnetics, IEEE Trans. Magn. 37(4), 1824-1826.
[5] Guo, X. C., Knigge, B., Marchon, B., Waltman, R. J., Carter, M., Burns, J. (2006). Multidentate functionalized lubricant for ultralow head/disk spacing in a disk drive. Journal of applied physics, 100(4), 044306.
[6] Gui, J. (2003). Tribology challenges for head-disk interface toward 1 Tb/in 2. Magnetics, IEEE Trans. Magn. 39(2), 716-721.
[7] Ma, X., Gui, J., Smoliar, L., Grannen, K., Marchon, B., Jhon, M. S., Bauer, C. L. (1999). Spreading of perfluoropolyalkylether films on amorphous carbon surfaces. The Journal of chemical physics, 110(6), 3129-3137.
[8] Jhon, M. S., Izumisawa, S., Guo, Q., Phillips, D. M., Hsia, Y. (2003). Simulation of nanostructured lubricant films. Magnetics, IEEE Trans. Magn. 39(2), 754-758.
[9] Waltman, R. J., Khurshudov, A., Tyndall, G. W. (2002). Autophobic dewetting of perfluoropolyether films on amorphous-nitrogenated carbon surfaces. Tribology Letters, 12(3), 163-169.
[10] Ma, X., Gui, J., Grannen, K. J., Smoliar, L. A., Marchon, B., Jhon, M. S., Bauer, C. L. (1999). Spreading of PFPE lubricants on carbon surfaces: effect of hydrogen and nitrogen content. Tribology Letters, 6(1), 9-14.
[11] Reiter, G. (1992). Dewetting of thin polymer films. Physical Review Letters, 68(1), 75.
[12] Xie, R., Karim, A., Douglas, J. F., Han, C. C., Weiss, R. A. (1998). Spinodal dewetting of thin polymer films. Physical Review Letters, 81(6), 1251.
[13] Seemann, R., Herminghaus, S., Jacobs, K. (2001). Dewetting patterns and molecular forces: A reconciliation. Physical Review Letters, 86(24), 5534.
[14] Redon, C., Brochard-Wyart, F., Rondelez, F. (1991). Dynamics of dewetting. Physical review letters, 66(6), 715.
[15] Becker, J., Grün, G., Seemann, R., Mantz, H., Jacobs, K., Mecke, K. R., Blossey, R. (2003). Complex dewetting scenarios captured by thin-film models. Nature Materials, 2(1), 59-63.
[16] Derjaguin, B. V., Churaev, N. V. (1974). Structural component of disjoining pressure. Journal of Colloid and Interface Science, 49(2), 249-255.
[17] Blossey, R. (2012). Thin liquid films: dewetting and polymer flow. Springer Science & Business Media.
[18] Scarpulla, M. A., Mate, C. M., Carter, M. D. (2003). Air shear driven flow of thin perfluoropolyether polymer films. The Journal of chemical physics, 118(7), 3368-3375.
[19] Marchon, B., Dai, Q., Nayak, V., Pit, R. (2005). The physics of disk lubricant in the continuum picture. Magnetics, IEEE Trans. Magn. 41(2), 616-620.
[20] Mate, C. M. (2013). Spreading kinetics of lubricant droplets on magnetic recording disks. Tribology Letters, 51(3), 385-395.
[21] Tani, H., Kubota, M., Tsujiguchi, Y., Tagawa, N. (2011). Visualization of lubricant pickup phenomena by lubricant thickness mapping on slider surface. Microsystem technologies, 17(5-7), 1175-1178.

[22] Mate, C. M., Marchon, B., Murthy, A. N., Kim, S. H. (2010). Lubricant-induced spacing increases at slider–disk interfaces in disk drives. Tribology letters, 37(3), 581-590.
[23] Wu, H., Mendez, A. R., Xiong, S., Bogy, D. B. (2015). Lubricant reflow after laser heating in heat assisted magnetic recording. Journal of Applied Physics, 117(17), 17E310.
[24] Gross, W. A., Matsch, L. A., Castelli, V., Eshel, A., Vohr, J. H., Wildmann, M. (1980). Fluid film lubrication (No. DOE/TIC-11301). John Wiley and Sons, Inc., New York, NY.
[25] Mendez, A. R., Bogy, D. B. (2014). Lubricant flow and accumulation on the slider's air-bearing surface in a hard disk drive. Tribology Letters, 53(2), 469-476.
[26] Sarabi, M. S. G., Bogy, D. B. (2014). Simulation of the Performance of Various PFPE Lubricants Under Heat Assisted Magnetic Recording Conditions. Tribology Letters, 56(2), 293-304.
[27] Karis, T. E., Marchon, B., Flores, V., Scarpulla, M. (2001). Lubricant spin-off from magnetic recording disks. Tribology Letters, 11(3-4), 151-159.
[28] Karis, T. E., Tyndall, G. W. (1999). Calculation of spreading profiles for molecularly-thin films from surface energy gradients. Journal of non-newtonian fluid mechanics, 82(2), 287-302.
[29] Marchon, B., Dai, Q., Knigge, B., Pit, R. (2007). Lubricant dynamics in the sub-nanometer clearance regime. Magnetics, IEEE Trans. Magn. 43(9), 3694-3698.
[30] Kubotera, H., Bogy, D. B. (2007). Numerical simulation of molecularly thin lubricant film flow due to the air bearing slider in hard disk drives. Microsystem technologies, 13(8-10), 859-865.
[31] Mate, C. M. (2011). Taking a fresh look at disjoining pressure of lubricants at slider-disk interfaces. Magnetics, IEEE Trans. Magn. 47(1), 124-130.
[32] Bowles, A. P., Hsia, Y. T., Jones, P. M., Schneider, J. W., White, L. R. (2006). Quasi-equilibrium AFM measurement of disjoining pressure in lubricant nano-films I: Fomblin Z03 on silica. Langmuir, 22(26), 11436-11446.
[33] Oron, A., Davis, S. H., Bankoff, S. G. (1997). Long-scale evolution of thin liquid films. Reviews of modern physics, 69(3), 931.
[34] Kim, H. I., Mate, C. M., Hannibal, K. A., Perry, S. S. (1999). How disjoining pressure drives the dewetting of a polymer film on a silicon surface. Physical review letters, 82(17), 3496.
[35] Evans, L. C. (1998). Partial Differential Equations, Graduate Studies in Mathematics, vol. 19, American Mathematical Society, Providence.
[36] Tyndall, G. W., Waltman, R. J., Pocker, D. J. (1998). Concerning the interactions between Zdol perfluoropolyether lubricant and an amorphous-nitrogenated carbon surface. Langmuir, 14(26), 7527-7536.
[37] http://cml.berkeley.edu/cmlair_new.html.
[38] Xu, L., Ogletree, D. F., Salmeron, M., Tang, H., Gui, J., Marchon, B. (2000). De-wetting of lubricants on hard disks. The Journal of Chemical Physics, 112(6), 2952-2957.